# Comparison between the transverse responses of the reactions $^{12}C(e, e'p)^{11}B$ and $^{12}C(\gamma, p)^{11}B$

S. A. Morrow,[1,*] J. Arneil,[1] E. C. Aschenauer,[2] M. F. van Batenburg,[2] H. P. Blok,[2,†] D. J. Boersma,[2] D. Branford,[1] T. Davinson,[1] G. DeMeyer,[3] J. E. Ducret,[4] W. H. A. Hesselink,[2,†] D. Groep,[2] K. Hicks,[2] D. G. Ireland,[5] N. Kalantar-Nayestanaki,[6] L. Lapikás,[2] M. Liang,[1] J. Mackenzie,[1] C. Marchand,[4] R. Medaglia,[4] J. Ryckebusch,[3] M. van Sambeek,[2,†] R. Starink,[2,†] G. van der Steenhoven,[2] M. A. van Uden,[2] and H. de Vries[2]

[1]*School of Physics, University of Edinburgh, Edinburgh EH9 3JZ, United Kingdom*

[2]*NIKHEF, P.O. Box 41882, NL-1009 DB Amsterdam, The Netherlands*

[3]*Department of Subatomic and Radiation Physics, University of Gent, Proeftuinstraat 86, B-9000 Gent, Belgium*

[4]*CEA–Saclay, Service de Physique Nucléaire, F-91191 Gif-sur-Yvette Cedex, France*

[5]*Department of Physics and Astronomy, University of Glasgow, Glasgow G12 8QQ, United Kingdom*

[6]*KVI, Rijksuniversiteit Groningen, NL-9747 AA Groningen, The Netherlands*

(Received 30 November 2003; published 26 January 2005)

A study of the reaction $^{12}C(e, e'p)^{11}B$ in parallel kinematics has been made for the missing-momentum region $250 < p_m < 310$ MeV/$c$ at incident energies of 379 and 585 MeV. A Rosenbluth separation of the cross sections was carried out to extract the longitudinal and transverse structure functions $W_L$ and $W_T$. Calculations that include meson-exchange currents and isobar currents are seen to describe the data better than those using a one-body current only. For the first time, a comparison between the $^{12}C(\gamma, p)$ cross section and the transverse part of the $^{12}C(e, e'p)$ cross section has been made versus an effective momentum that is defined in such a way as to minimize effects due to differences in final-state interactions. This comparison suggests that it may be possible to describe both reactions in one consistent framework if two-body currents are included.

DOI: 10.1103/PhysRevC.71.014607 PACS number(s): 24.10.Eq, 25.20.Lj, 25.30.Rw, 27.20.+n

## I. INTRODUCTION

Many experiments on single-proton knockout from nuclei have been performed above the giant resonance region with electromagnetic probes, using both real and virtual photons (see, for example, Refs. [1–9]). On the one hand, in quasi-elastic kinematics, the $(e, e'p)$ results are well described assuming a direct-knockout (DKO) mechanism, provided that low missing energies and missing momenta below the Fermi momentum are probed. Under those conditions, the $(e, e'p)$ process can be used to obtain detailed information on single-particle bound-state wave functions (BSWF) and spectroscopic factors. On the other hand, the magnitudes of the $(\gamma, p)$ data are poorly described by nonrelativistic DKO calculations, the experimental results being higher, by a factor of 2 to 10, than the DKO calculations for nuclei in the range $A = 9$ to 209 [6–9]. Also, the $(\gamma, p)$ reaction is observed in some cases to excite more complicated states than the one-hole $(1h)$ states, which are dominantly excited by DKO, suggesting a more complex reaction mechanism than DKO.

Numerous reaction mechanisms and kinematic effects have been considered to explain the anomalously high $(\gamma, p)$ reaction strength, such as (i) photon absorption on p–n pairs, as parametrized by the quasi-deuteron model (QDM) [10], (ii) photon absorption on $T = 1$ p–n pairs [11,12], (iii) coupled-channel (two-step) processes [13], (iv) relativistic effects [14–18], and (v) photon absorption on a nucleon pair via meson-exchange currents [19,20]. The latter calculations appear to give the most successful description of the data.

An interesting experimental result provided by the electromagnetically induced single-proton knockout reactions is that in almost all cases the $(\gamma, p)$ and $(e, e'p)$ reactions on the same nucleus give rise to nearly equal relative populations of states in the residual nucleus. This is somewhat surprising since most $(e, e'p)$ data have been taken in a kinematics that emphasizes the longitudinal response, whereas the $(\gamma, p)$ reaction involves purely transverse photons, which may indicate that there is some nontrivial connection between the two mechanisms. However, in one specific case, that of $^{12}C$, a marked difference was observed between the two sets of experimental data available. The $^{12}C(\gamma, p)$ data show a strong cross section for excitation of the residual nucleus, $^{11}B$, at ~7-MeV excitation energy [11,21–26], which is only very weakly seen in the $^{12}C(e, e'p)$ data. The three states involved have excitation energies of 6.74 MeV $(7/2^-)$, 6.79 MeV $(1/2^+)$, and 7.29 MeV $(5/2^+)$ in $^{11}B$ [27].

The observed difference between the two reactions has generated considerable interest, both experimental and theoretical, in the $^{12}C(e, e'p)^{11}B$ and $^{12}C(\gamma, p)^{11}B$ reactions. However, all investigations suffered from two problems: (i) the inability to determine experimentally which members of the 7 MeV triplet of states in $^{11}B$ are excited by the reaction $^{12}C(\gamma, p)^{11}B$ and in what proportions; and (ii) the momentum values probed and the relative contributions of longitudinal and transverse responses are rather different among existing $^{12}C(e, e'p)^{11}B$ and $^{12}C(\gamma, p)^{11}B$ data. Recently, two experiments [20,28] (both performed using the $(\gamma, p\gamma')$ technique) succeeded in resolving the first problem. The result showed that the $7/2^-$ state carries most strength in the tripet, a result in agreement

*Electronic address: s.a.morrow@physics.org; present address: CEA–Saclay, Service de Physique Nucléaire, F-91191 Gif-sur-Yvette Cedex, France.

†Also at Vrije Universiteit, De Boelelaan 1081, NL-1081 HV Amsterdam, The Netherlands.

 

with the two-step calculations of [13] and the predictions of the model [19,20] whereby the photon is absorbed on an exchange current. The overall strength of the ~7-MeV triplet, however, no matter which state is responsible, is still high when compared to the $^{12}$C$(e, e'p)$ data.

In order to study the unexplained difference between the two reactions, this work focused on extending the previous $(e, e'p)$ measurements and improving the comparison between the data sets for each of the two reactions. To make a more thorough comparison, an attempt has been made to overcome the two main discrepancies between the data sets when they were compared previously in [8]. These discrepancies were: (i) the $^{12}$C$(e, e'p)^{11}$B and $^{12}$C$(\gamma, p)^{11}$B data were not taken at the same missing momentum $p_m$; and (ii) the $^{12}$C$(e, e'p)^{11}$B data included both longitudinal and transverse components in the cross section.

This paper presents new results for the $^{12}$C$(e, e'p)^{11}$B reaction. A longitudinal–transverse separation of the reaction cross section has been performed for $250 < p_m < 310$ MeV/$c$, a range in which there are $^{12}$C$(\gamma, p)^{11}$B data for all states in the discrete part of the $^{11}$B spectrum. By extracting the transverse structure function, a comparison of the electron-induced reaction with the existing $^{12}$C$(\gamma, p)^{11}$B data is made possible. The only differences remaining are the final-state interactions and the energy of the incident (virtual) photon.

This paper is organized as follows: in Sec. II the necessary formalism of the $(e, e'p)$ reaction is presented. In Sec. III the experimental setup and data analysis are described. The results of the present measurement are discussed in Sec. IV. In Sec. V the $(e, e'p)$ and the $(\gamma, p)$ data are compared. Conclusions are presented in Sec. VI.

## II. THEORETICAL BACKGROUND

Reduced cross sections and structure functions were determined from the measured cross sections using analysis methods based on the plane-wave impulse approximation (PWIA). These results are compared to theoretical calculations obtained using the distorted-wave impulse approximation (DWIA) and the random-phase approximation (RPA).

In the PWIA, the $(e, e'p)$ cross section may be factorized into a term representing the elementary electron-proton scattering cross section $\sigma_{\rm ep}$ and the spectral function $S(E_m, p_m)$. The spectral function represents the probability of finding a proton within the target nucleus with a removal energy $E_m$ and an initial momentum $p_m$. In the PWIA, it is related to the sixfold differential cross section via

$$\frac{d^6\sigma}{dE_{e'}\,d\Omega_{e'}\,dE_p\,d\Omega_p} = K\sigma_{\rm ep}S(E_m, p_m), \qquad (1)$$

where $E_{e'(p)}$ and $\Omega_{e'(p)}$ are, respectively, the energies and detection solid angles of the electron (proton), and $K = p'E_p$, where $p'$ is the momentum of the outgoing proton.

If neither the beam nor the target is polarized, the sixfold cross section may be expressed in terms of four structure functions $W_L$, $W_T$, $W_{\rm TT}$, and $W_{\rm LT}$ [29]. When the measurement is made in parallel kinematics, the number of structure functions is reduced to two [30]. The sixfold differential cross section may then be written as

$$\frac{d^6\sigma}{dE_{e'}\,d\Omega_e\,dE_p\,d\Omega_p} = K\sigma_{\rm Mott}\frac{Q^2}{q^2}\{\epsilon^{-1}W_T + W_L\}, \qquad (2)$$

where $K$ is as defined in (1), $\sigma_{\rm Mott} = \{\frac{\alpha\cos(\theta_{e'}/2)}{2E_0\sin^2(\theta_{e'}/2)}\}^2$ is the Mott cross section, and $Q^2 = q^2 - \omega^2$, where $q$ is the 3-momentum transfer and $\omega$ is the energy transfer. The longitudinal photon polarization parameter $\epsilon$ is given by $\epsilon = \{1 + 2(\frac{q^2}{Q^2})\tan^2(\theta_{e'}/2)\}^{-1}$ and determines the longitudinal–transverse character of the exchanged virtual photon. It may vary from 0 to 1, where $\epsilon = 1\,(=0)$ implies a purely longitudinal (transverse) photon. From measurements of the cross section at two beam energies, where $E_p$, $\omega$, and $q$ have been kept constant by the choice of kinematics, an extraction of the structure functions $W_L$ and $W_T$ is possible (via Rosenbluth separation).

The DWIA calculations were made using a nonrelativistic, unfactorized complete DWIA code (CDWIA) based on the paper by Boffi *et al.* [31]. These calculations include Coulomb distortions of the electron waves. The proton final-state interactions (FSI) are taken into account through the use of distorted waves derived from phenomenological proton optical-model potentials. Contributions to the $(e, e'p)$ cross sections from initial virtual-photon absorption on a neutron followed by charge exchange and scattering processes were considered previously in Ref. [32] and found to be negligible compared to the direct processes. Reaction processes involving an initial absorption of a virtual photon on a neutron are therefore not included in the CDWIA code. The inclusion of a spin dependence in the potentials determining the distorted waves destroys the simple factorized expression for the cross section; i.e., it can no longer be separated into a nuclear structure part [the spectral function $S(E_m, p_m)$] and an electron-nucleon interaction part. Nevertheless, it is possible to *define* a distorted spectral density function, obtained by dividing the measured and computed cross sections by $K\sigma_{\rm ep}$. This is a very useful quantity to use in comparisons between theory and data, and between various data sets. As all theoretical calculations presented in this paper have been obtained in an unfactorized approach including spin-orbit effects, the representation of data and calculations in terms of a distorted spectral function does not involve any approximation.

The RPA calculations were made using the model of [33]. In this model, the incoming photon is considered to interact with all individual nucleons in the target nucleus. A nucleon photoexcited into a continuum state interacts with the remaining A-1 nucleons via the mean field and residual interactions. Wave functions are constructed for the final state that permit the required one-particle emission, allowing the residual nucleus to be left in a $(1h)$ state, with a proton in the continuum. In this model both initial-state nuclear correlations and all particle–hole diagrams contributing to the FSI are taken into account. The RPA model respects unitarity and allows multistep processes, such as photon absorption on a neutron followed by charge exchange or scattering. This is different from the classical DWIA *quasi–free* knockout picture. However, since intermediate states beyond the typical RPA diagrams are not included, this means that only part of

the absorptive effects is implemented. In the giant resonance region the effect of diagrams beyond the RPA ones induces a serious spreading of the strength. Indeed, higher-order diagrams are usually linked to the collective properties of the target nucleus. The effect of collective properties decreases with increasing energy and is considered to be small for the energies ($T_p \sim 175$ MeV) considered in this work, which are far above the giant resonance domain.

Just as in the DWIA model, the standard RPA approach is restricted to single-nucleon ejection to states with a predominant $(1h)$ character relative to the ground state of the target nucleus. However, it was shown [19] that, by adding two-body currents to the calculation [33], the possibility of populating two-hole one-particle $(2h1p)$ states in the residual (A-1) nucleus is included. This approach was used to explain the population of states at ~7 MeV in $^{11}$B following $^{12}$C$(\gamma, p)$. In this picture, two nucleons are removed from their shell-model orbitals, but whereas one remains bound in a higher excited state, the other escapes to the continuum. Such a process could be looked upon as a "prethreshold" two-nucleon emission process, with one ejected particle and a second nucleon that is excited into an unoccupied but bound level above the Fermi level of the mean-field potential.

Both the DWIA model [31] and the RPA model [33] were used to calculate structure functions in addition to the reduced cross sections.

## III. EXPERIMENTAL METHOD AND ANALYSIS

The experiment was carried out at the EMIN hall [34] electron-scattering facility at NIKHEF (National Institute for Nuclear Physics and High-Energy Physics). The electron beam was delivered by the AmPS (Amsterdam Pulse Stretcher) ring [35]. Beam energies of $E_0 = 378.5 \pm 0.4$ and $585.1 \pm 0.6$ MeV were used. The duty factor was ~50% and ~75%, in the measurements at low- and high-beam energy, respectively. The average beam current was about 10 $\mu$A. Natural carbon targets were used. A single ($102.9 \pm 2.6$ mg/cm$^2$) and a triple foil target ($3 \times 34.3 \pm 0.9$ mg/cm$^2$, separated by 4 mm each) were used in the measurements at low- and high-beam energy, respectively. These targets were also used for the energy calibration of the electron beam via elastic and inelastic scattering.

The scattered electrons and the knocked-out protons were detected in two magnetic spectrometers: a high-resolution ($\Delta p/p \sim 1 \times 10^{-4}$; $\Delta\Omega = 5.54$ msr) quadrupole-dipole-dipole (QDD) spectrometer for the electrons and a quadrupole-dipole-quadrupole (QDQ) spectrometer with a larger solid angle ($\Delta p/p \sim 2 \times 10^{-4}$; $\Delta\Omega = 15.91$ msr) for the protons. The coincidence–time resolution between these spectrometers was about 1 ns. A detailed description of the EMIN scattering facility, the spectrometers, and the data acquisition can be found in Refs. [34,36].

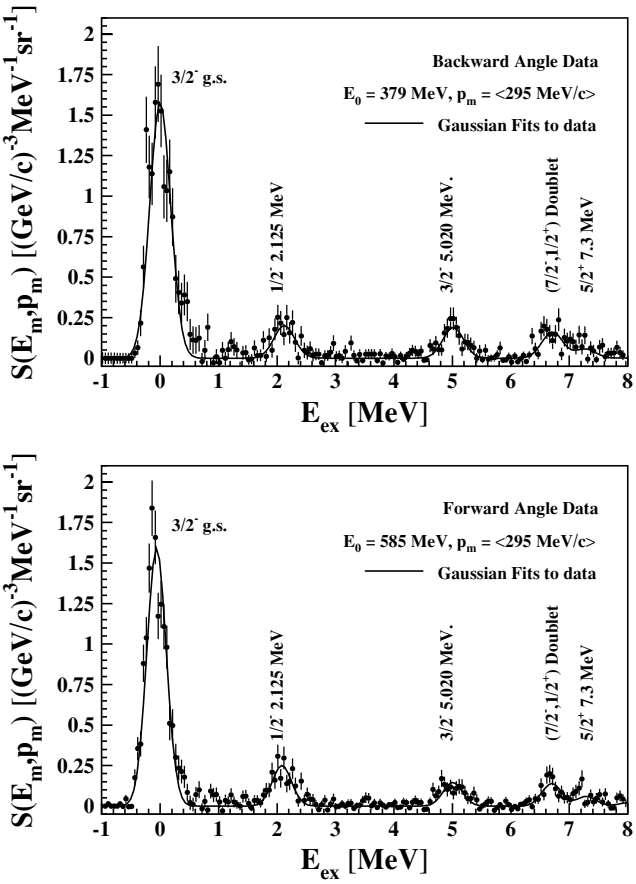


FIG. 1. $^{12}$C$(e, e'p)$ excitation spectra for the measurements at high- and low-beam energy, in terms of the spectral function, $S(E_m, p_m)$. The data were taken over a 10-MeV/$c$ bin with its center at $p_m$ of 295 MeV/$c$. The $E_x$ resolution is ~450 keV full width half maximum (FWHM).

Typical excitation energy $E_x$ spectra from the current data set are shown in Fig. 1. The many existing data sets available from NIKHEF show much better $E_m$ resolution than that achieved here. The poorer resolution of the current data (around 450 keV) is explained by proton energy losses in the rather thick target (see Table I), which was used in order to increase statistics for the weakly excited states. Data

TABLE I. Central kinematics for each of the measurements.

| $p_m$ ($\frac{\text{MeV}}{c}$) | $q$ ($\frac{\text{MeV}}{c}$) | $\theta_{e'}$ (deg) | $\theta_p$ (deg) | $t_{\text{tg}}$ ($\frac{\text{mg}}{\text{cm}^2}$) | $E_0$ (MeV) | $\epsilon$ |
|---|---|---|---|---|---|---|
| 259.9 | 338.2 | 63.2 | −28.5 | 102.9 | 378.55 | 0.47 |
| 299.8 | 298.3 | 50.5 | −27.7 | 102.9 | 378.55 | 0.55 |
| 257.9 | 338.4 | 33.5 | −39.2 | $3 \times 34.3$[a] | 585.10 | 0.78 |
| 298.5 | 298.6 | 27.1 | −36.1 | $3 \times 34.3$[a] | 585.10 | 0.83 |

[a]These measurements were made with a triple foil target.

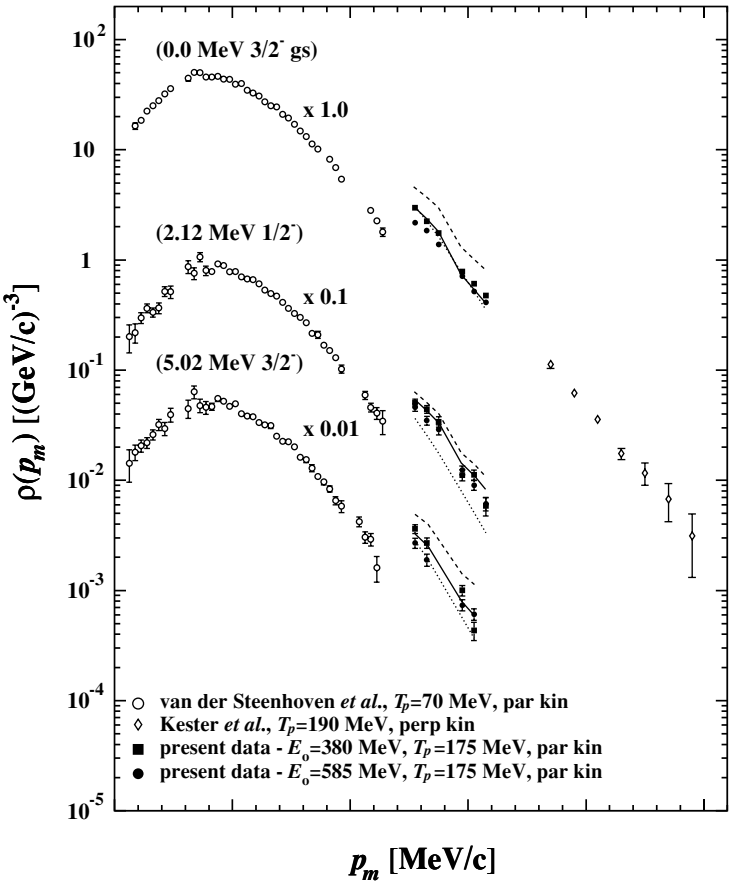


FIG. 2. Momentum distributions for the ground state 2.12- and 5.02-MeV transitions, corresponding to $1p$ knockout from $^{12}$C. Open circles represent the data of van der Steenhoven *et al*. [40], and open diamonds represent the data of Kester *et al*. [42]. The solid data points are from the current experiment. Solid squares represent the data with a beam energy of 378.5 MeV; solid circles represent the data with a beam energy of 585.1 MeV. See the text for details of the theory results shown. The current data are shown with statistical errors only. The mismatch in normalization between the $T_p \geqslant 175$ MeV and $T_p = 70$ MeV data sets is explained in the text. "Par kin" stands for parallel kinematics, "perp kin" for perpendicular kinematics.

were accumulated in parallel (coplanar) kinematics in the $p_m$ range of ∼250–310 MeV/$c$. Parallel kinematics refers to the restricted case where the momentum of the emitted proton $p'$ is parallel to the momentum transfer $q$. Coplanar kinematics implies that the scattering and reaction planes coincide. A series of four measurements (in two pairs, each pair with a different beam energy) was made at two central missing momentum values, ∼260 and ∼300 MeV/$c$. The knocked-out protons had energies centered around $T_p =$ 175 MeV in all measurements. The main parameters of each run are shown in Table I.

The $(e, e'p)$ analysis presented here consisted of extracting the spectral functions, the momentum distributions, and from a Rosenbluth separation, the structure functions $W_L$ and $W_T$. The basic procedure used for analysis of $(e, e'p)$ data at NIKHEF to obtain momentum distributions is described in detail in Refs. [36,37] and is briefly summarized below.

For an electron-proton coincidence, the difference in the arrival times at each of the two spectrometers was measured and then corrected for the time-of-flight. A time-coincidence window was applied to the corrected QDD-QDQ time, an $E_m$ histogram was created for this cut, and the accidental coincidences were subtracted. The acceptance as a function of $E_m$ and $p_m$ for the detection of electron-proton coincidences was determined with a Monte Carlo simulation. This allowed a calculation of the sixfold differential cross section $\sigma^{\rm exp}$. The data were corrected for radiative effects using the method described in [36]. Furthermore, the factor $K\sigma_{\rm ep}$ (using the definition $\sigma_{\rm ep}^{\rm cc1}$ of de Forest [38]) was accounted for on an event-by-event basis, allowing extraction of the reduced cross section $\sigma^{\rm red}(E_m, p_m) = \sigma^{\rm exp}/K\sigma_{\rm ep}$.

From the experimental reduced cross sections, momentum distributions $\rho(p_m)$ were extracted for each transition according to $\rho(p_m) = \int_{\Delta E_m} \sigma^{\rm red}(E_m, p_m)\, dE_m$. The spectra were fitted with 5 Gaussian peaks (as shown in Fig. 1) and, for all states, the peak areas were determined by summing the actual experimental bin content within $\pm 2\sigma$ of the peak position. For the partially resolved states, the $(1/2^+, 7/2^-)$ doublet, and the 7.3-MeV state, the fitted Gaussian tails from neighboring overlapping peaks were also subtracted. In view of the peak-shape dependence of this procedure a 15% systematic error has been assigned to the experimental cross sections for these two states.

The $p_m$ bins were chosen to be 10 MeV/$c$ wide, a compromise between statistical precision per bin and the $(\omega, q)$ acceptance within one bin. The finite acceptance within one bin leads to events that are not in perfectly parallel kinematics. These finite acceptance effects were taken into account, according to the method of [39], before making the longitudinal–transverse separation. The effects of nonparallel contributions (predominantly arising from the interference structure function $W_{\rm LT}$) have been considered and are assumed to be small for two reasons. First, the size of $W_{\rm LT}$ relative to $W_L$ is of order $\sin(\theta_{\rm pq})$, where $\theta_{\rm pq}$ is the angle between the vectors $\mathbf{p}'$ and $\mathbf{q}$. In the present parallel kinematics this angle is smaller than a few degrees due to the limited acceptances

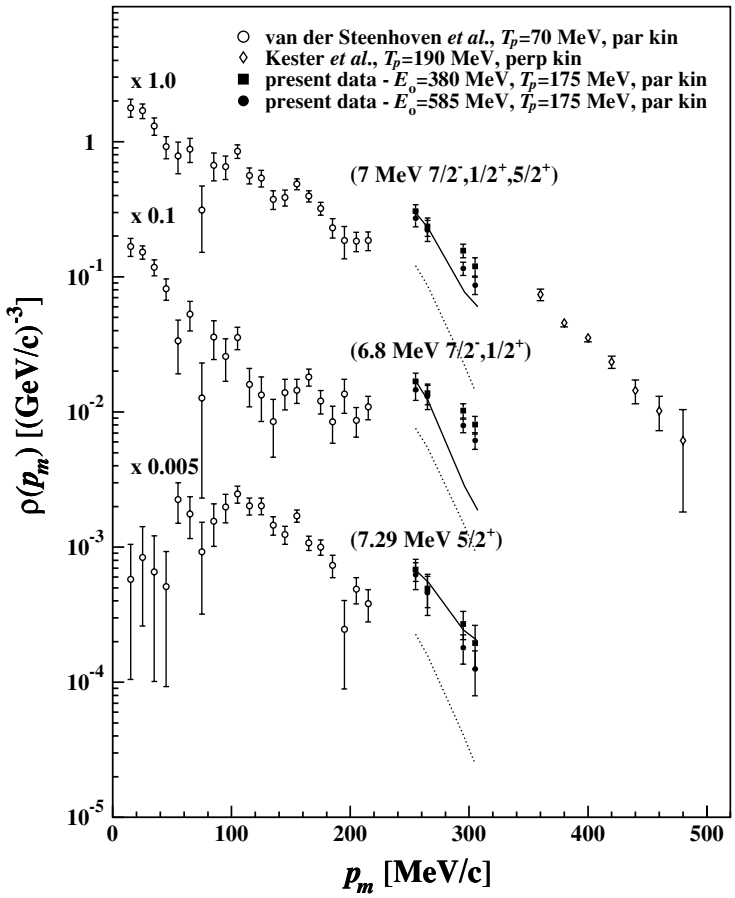


FIG. 3. Momentum distributions for transitions to the states in the 7-MeV triplet. See Fig. 2 for a description of the experimental data and theory results displayed. The current data are shown with statistical errors only. The mismatch in normalization between the $T_p \geqslant 175$ MeV and $T_p = 70$ MeV data sets is explained in the text. "Par kin" stands for parallel kinematics, "perp kin" for perpendicular kinematics.

of the spectrometers. Second, since $W_{\rm LT}$ is proportional to $\sin(\theta_{\rm pq})$, its contribution to the cross section in a bin will practically average out to zero. This is because the centers of all bins were chosen to correspond to $\theta_{\rm pq} = 0$, and hence the contributions from positive and negative values of $\theta_{\rm pq}$, which are equally probable in parallel kinematics, cancel each other. In view of these considerations, we considered nonparallel effects to be negligible and this is assumed in the following.

The structure functions, $W_L$ and $W_T$, were deduced from the measured cross sections at the two beam energies via a Rosenbluth separation according to Eq. (2). The statistical and systematic errors on the cross sections were propagated through the separation procedure.

The total systematic error in the reduced cross sections for the resolved states was estimated to be ∼4%, which is comparable to the systematic errors quoted for several earlier $^{12}$C$(e, e'p)^{11}$B measurements made with the EMIN facility [40–43]. The absolute normalization of the present data was checked against previous $^{12}$C$(e, e'p)$ data [40] via two dedicated runs at outgoing proton energies of $T_p = 70$ and 85 MeV, with the same experimental setup. As described in detail in [41] the resulting spectroscopic factors for the g.s. transition agree within 2% with the previous data. Although in the analysis of the higher excited states the systematic errors of 15% on the cross sections were taken into account, the final errors associated with individual data points are still dominated by statistical uncertainties.

## IV. RESULTS

An overview of the NIKHEF data sets on the reaction $^{12}$C$(e, e'p)$ in parallel kinematics, including the current data, is shown in Figs. 2 and 3. The momentum distributions $\rho(p_m)$ as measured in the current experiment (for beam energies of 378.5 and 585.1 MeV) are plotted alongside previous data of van der Steenhoven *et al.* [40] and Kester *et al.* [42]. The missing-momentum range of the present experiment spanned a region between these two existing data sets. Also shown are theory calculations corresponding only to the high-energy kinematics of the current data set.

The lack of a smooth connection between the data of each separate experiment is due to the difference in kinetic energy of the emitted proton. The data of Ref. [40] were taken at $T_p =$ 70 MeV. This corresponds to a situation where the outgoing protons are expected to experience larger FSI than for both the current measurement and that of Ref. [42], which had $T_p =$ 175 and 190 MeV, respectively. Arguments based on proton FSI are also able to explain why the match (for the ground state and ∼7-MeV triplet transitions) between the current data and those of Ref. [42] is much better than between the current data and those of Ref. [40].

In Figs. 4 and 5 the current momentum distributions for the two different beam energies are compared on a linear scale to the two different calculations. In Figs. 6 and 7 the separated structure functions are displayed. Especially in the latter case, it can be seen that the error bars are

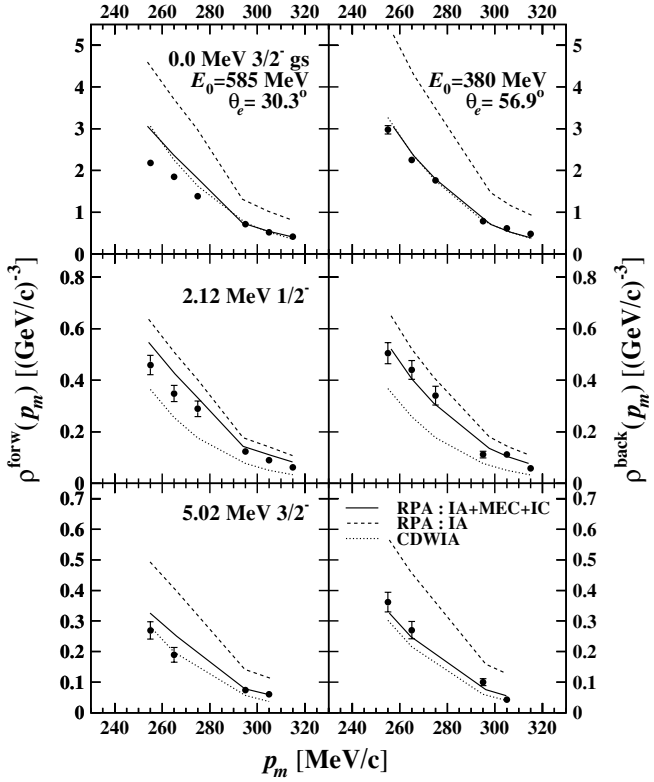


FIG. 4. Momentum distributions for the strong $1p$ transitions to states in $^{11}$B. RPA calculations [33] are shown with (solid lines) and without (dashed lines) MEC and IC. The dotted lines represent CDWIA calculations (see the text for details). The spectroscopic factors employed for these calculations are shown in Table III. The data are shown with statistical errors only. $\rho^{\text{forw}}$ and $\rho^{\text{back}}$ represent the momentum distributions measured at the forward angle ($E_0 = 585$ MeV) and backward angle ($E_0 = 380$ MeV) settings, respectively.

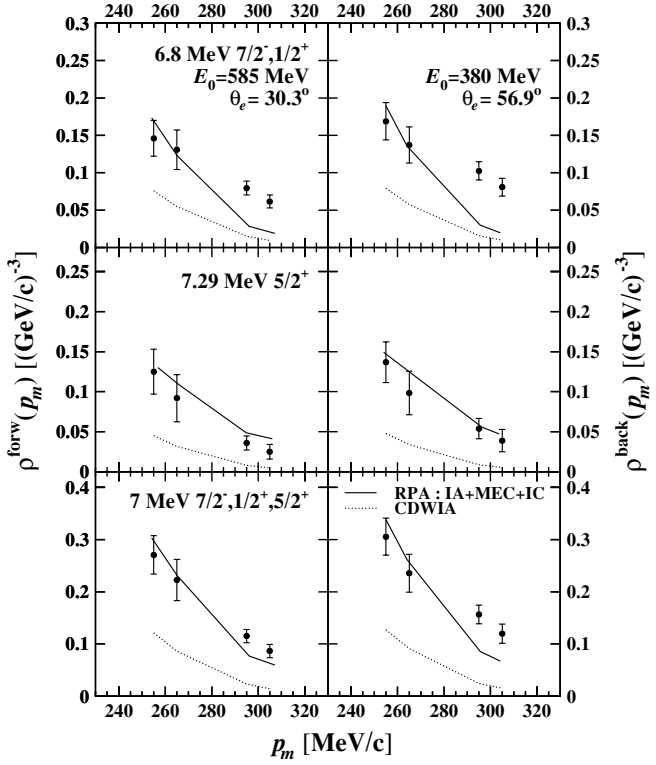


FIG. 5. Momentum distributions for weak transitions to states around 7 MeV in $^{11}$B. See Fig. 4 for an explanation of the different lines in the plot. The spectroscopic factors employed for the calculations are shown in Table III. The data are shown with statistical errors only. The data are shown with statistical errors only. $\rho^{\text{forw}}$ and $\rho^{\text{back}}$ represent the momentum distributions measured at the forward angle ($E_0 = 585$ MeV) and backward angle ($E_0 = 380$ MeV) settings, respectively.

enlarged due to the longitudinal–transverse separation procedure. The data are compared to CDWIA calculations [31] and calculations in the RPA framework [33], both with and without meson-exchange currents (MEC) and Δ-Isobar (IC) contributions.

The results of the CDWIA calculations are displayed as the dotted lines in Figs. 4 and 5. The calculations were made using a code including an approximate treatment of the distortion of the electron waves due to the Coulomb field of the nucleus. Also, the FSI between the outgoing proton and the residual (A-1) nucleus is taken into account. This is done by distorting the proton wave with a (nonrelativistic) optical-model potential. This potential is taken from an analysis [44] of elastic proton-scattering data, and parametrized as a function of $T_p$. See Table II for the potential parameters used in the current calculations.

The range of $p_m$ covered in the current experiment was not sufficient for an independent determination of $S_\alpha$ and $r_{\text{rms}}$ within a complete analysis with the CDWIA. Therefore, spectroscopic factors $S_\alpha$ and the root-mean-square radii $r_{\text{rms}}$ of the bound-state wave functions for each state were taken from [41]. In these analyses, the $r_{\text{rms}}$ values were fitted by keeping the potential well depth ($V_0$) and diffuseness parameter ($a_0$) of the Woods-Saxon potential constant. The value of $a_0$ was fixed at 0.65 fm for all states. Table III lists the values of $S_\alpha$ and $r_0$ used for the current analysis and the corresponding $r_{\text{rms}}$ values.

Calculations were also made for the $(e, e'p)$ cross section in the RPA model [33], with and without the inclusion of virtual-photon coupling to two-body currents. The two-body current operators included both MEC and IC contributions. The results are shown in Figs. 4 and 5, respectively. The dashed lines represent the result of the calculations accounting for one-body currents only. The solid lines represent the result of including the two-body currents. The two-body current calculations for the ∼7-MeV triplet states were made according to a procedure (outlined in [20]) whereby the overlap between the initial-state and the final-state wave function has $(1h)$ and $(2h1p)$ components, constructed as

$$\alpha|(1h)\rangle + \beta|(2h-1p)\rangle, \tag{3}$$

where $\alpha$ is determined by the spectroscopic factor $S_\alpha$, again taken from [40], and the parameter $\beta$ comes from shell-model calculations.

As with the CDWIA calculations, the RPA structure functions are shown in Figs. 6 and 7. When neglecting the

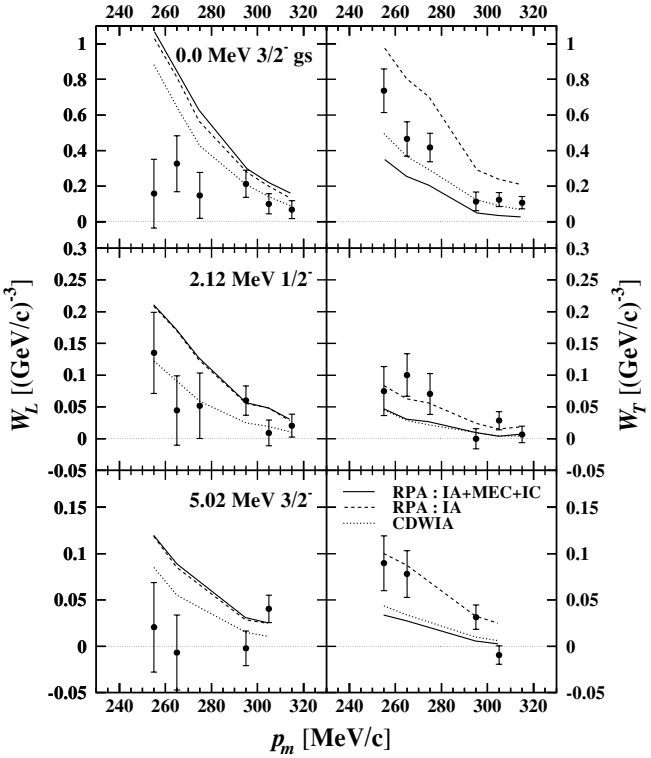


FIG. 6. Structure functions $W_L$ and $W_T$ for the strong $1p$ transitions to states in $^{11}$B, against $p_m$. See Fig. 4 for an explanation of the different lines in the plot. The data are shown with both statistical and systematic errors.

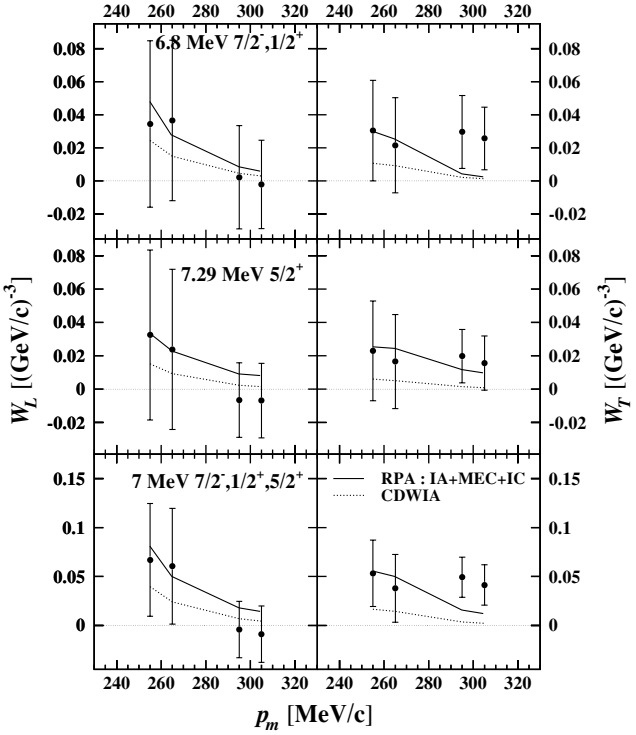


FIG. 7. Structure functions $W_L$ and $W_T$ for the weak transitions to states around 7 MeV in $^{11}$B, against $p_m$. See Fig. 4 for an explanation of the different lines in the plot. The data are shown with both statistical and systematic errors.

MEC and IC, the $(2h1p)$ contribution vanishes, leaving only the $(1h)$ contribution. The $(1h)$ contribution represents the population of orbitals above the Fermi surface for the states at ∼7 MeV. Within the context of the adopted model, the presence of a $(1h)$ contribution explains the nonvanishing longitudinal structure function calculated for the triplet states. The $(2h1p)$ wave-function components, being excited through the two-body currents, induce solely transverse strength.

From Figs. 4 and 5 it can be seen that the CDWIA calculations agree reasonably well with the results for the ground and 5.02-MeV $(3/2^-)$ excited states, whereas they underestimate the data for the 2.12-MeV $(1/2^-)$ state and the ∼7-MeV states. The RPA calculations including MEC and IC agree reasonably well with the data for all the states. This is consistent with the assumption made previously that the $3/2^-$ states are predominantly $(1h)$ states excited by DKO, whereas the $1/2^-$- and ∼7-MeV triplet states have more complicated structures such as $(2h1p)$, which are excited through virtual-photon absorption on MEC and IC. Despite the considerably improved description of the ∼7-MeV triplet states obtained with the RPA calculations, deviations remain visible for the 6.8-MeV state at $p_m$ ∼300 MeV/$c$, where the calculations systematically underestimate the data.

The structure function results shown in Figs. 6 and 7 tend to support the conclusions derived from the momentum distributions, but there are some differences. Whereas the $W_L$ and $W_T$ results for the $(1h)$ states in general are better reproduced by the CDWIA calculations, the longitudinal strength at 265 MeV/$c$ is somewhat overestimated for the $3/2^-$ states. The results for the triplet states are somewhat better described by the RPA calculations including MEC and IC, but the large error bars preclude us from drawing stronger conclusions.

## V. COMPARISON TO EXISTING $^{12}$C($\gamma$, $p$)$^{11}$B DATA

The initial motivation for the new measurements described here was to investigate unexplained experimental results in $^{12}$C$(\gamma, p)$ data. To consider these, a comparison has been made between the experimental data sets for the two

TABLE II. Optical-model potential parameters for $T_p = 175$ MeV protons employed in the CDWIA calculations.

| $V_0$ (MeV) | $r_0$ (fm) | $a_0$ (fm) | $W$ (MeV) | $r$ (fm) | $a$ (fm) | $V_{so}$ (MeV) | $r_{so}$ (fm) | $a_{so}$ (fm) |
|---|---|---|---|---|---|---|---|---|
| 6.571 | 1.2 | 0.686 | 14.478 | 1.156 | 0.603 | 3.054 | 0.899 | 0.447 |

TABLE III. The values of $r_0$, and the $r_{\rm rms}$ and $S_\alpha$ taken from [40], used in the CDWIA calculations.

| $J^\pi$ | $E_{\rm ex}$ (MeV) | $r_0 \times A^{1/3}$ (fm) | $r_{\rm rms}$ (fm) | $S_\alpha$ |
|---|---|---|---|---|
| $3/2^-$ | 0.00 | 3.1448 | 2.724 | 1.900 |
| $1/2^-$ | 2.12 | 3.9378 | 2.945 | 0.235 |
| $3/2^-$ | 5.02 | 3.5730 | 2.804 | 0.200 |
| $7/2^-$ | 6.74 | 5.5090 | 4.295 | 0.0038 |
| $1/2^+$(1s) | 6.79 | 1.0431 | 1.894 | 0.0031 |
| $1/2^+$(2s) | 6.79 | 4.8330 | 3.527 | 0.018 |
| $5/2^+$ | 7.29 | 4.5457 | 3.525 | 0.017 |

reactions $^{12}$C$(e, e'p)^{11}$B and $^{12}$C$(\gamma, p)^{11}$B. In Fig. 8, the current $^{12}$C$(e, e'p)$ data are presented as a "transverse reduced cross section", which has been defined as $W_T/F_T$, where

$$F_T(Q^2) = \left(Q^2/4{m_p}^2\right)\left(G_M^p(Q^2)\right)^2, \tag{4}$$

and $G_M^p$ is the proton magnetic form factor. These have been plotted alongside the $^{12}$C$(\gamma, p)$ data of Ruijter *et al.* [25], which have been converted from angular distributions to reduced cross sections according to the procedure suggested by [8]. The transformation (which only strictly holds in PWIA) is given by

$$\sigma_{\gamma p} \equiv \frac{d\sigma}{d\Omega} = K\frac{2\pi^2\alpha}{qm_p^2}\left(\mathbf{p}'^2_{c.m.}\sin^2\theta_p + \frac{1}{2}g_p^2\mathbf{q}^2\right)|\phi_\alpha(p_m)|^2 = C|\phi_\alpha(p_m)|^2, \tag{5}$$

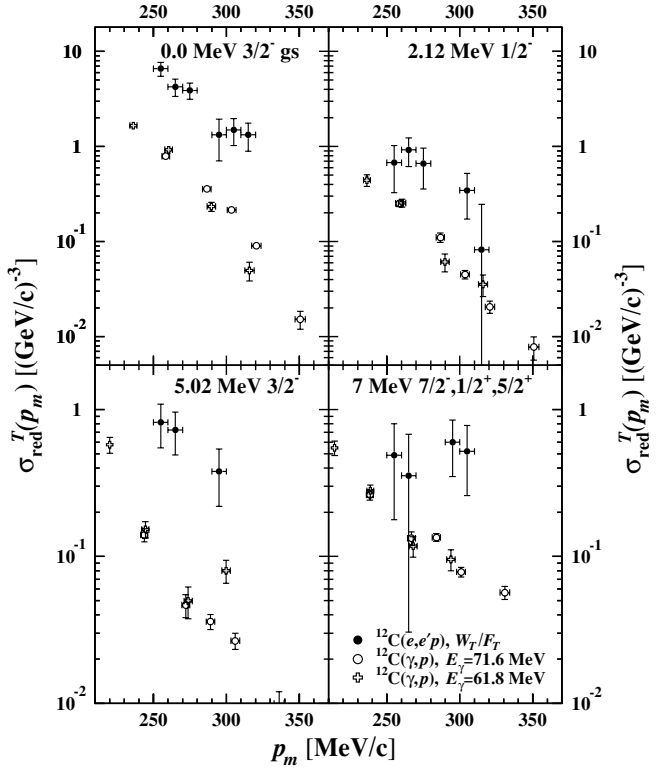


FIG. 8. Comparison of the transverse reduced cross sections for the present $(e, e'p)$ data with the four resolved transitions in the reaction $^{12}$C$(\gamma, p)$ of Ruijter *et al.* [25], as a function of $p_m$.

where $K$ is the kinematic factor defined in Sec. II. In PWIA, the transverse reduced cross section $\sigma^T_{\rm red}$, which equals $W_T/F_T$ for $(e, e'p)$ and $\sigma_{\gamma p}/C$ for $(\gamma, p)$, corresponds to the square of the radial overlap wave function in momentum space.

The comparison is shown for the three resolved $(1p)$ transitions and for the ∼7-MeV triplet. The top left and top right panels of Fig. 8 show results for the 0.0-MeV ground state and 2.12-MeV 1st excited states, respectively. The 4.45- and 5.02-MeV states, which are unresolved in the $(\gamma, p)$ data, are shown in the bottom left panel. The 4.45-MeV state has not been observed in $(e, e'p)$ experiments in parallel kinematics [40] but was observed in a dedicated experiment [43] in $(q, \omega)$ constant kinematics. The three unresolved states of the ∼7-MeV triplet are shown in the bottom right panel. Clearly, the data in Fig. 8 do not reveal consistency between reduced cross sections derived from $(e, e'p)$ and $(\gamma, p)$ data.

The differences observed between the $^{12}$C$(e, e'p)^{11}$B and $^{12}$C$(\gamma, p)^{11}$B results shown in Fig. 8 could be due to FSI effects, different reaction mechanisms, or both. In order to compare the two data sets on an equal footing, one should analyze the data in such a way as to remove effects that arise from the different $T_p$ values at which each measurement was made. This is clearly a worthwhile objective, since a difference in these $T_p$ values leads to each data set having a different sensitivity to the FSI effects. The $T_p$ of the $(\gamma, p)$ data shown is ∼50 MeV, whereas the $T_p$ for the current $(e, e'p)$ data is ∼175 MeV. To compensate for this difference, both data sets have been reanalyzed to produce plots of cross sections as a function of an effective transfered momentum $p_m^{\rm eff}$, where the quantity $\mathbf{p}_m^{\rm eff} = \mathbf{p}'^{\rm eff} - \mathbf{q}$ was calculated using the following effective proton momentum:

$$p'^{\rm eff} = p'\sqrt{1 + \frac{V_0}{T_p}}. \tag{6}$$

In this equation, $V_0$ represents the potential well from which the exiting proton must escape to leave the target nucleus. The potential used for $V_0$ was the real part of the optical potential used in the CDWIA calculations to describe the FSI effect, which is $T_p$ dependent. The results of this reanalysis are shown in Fig. 9.

Although the above procedure accounts for the largest FSI effects, it neglects changes in proton flux due to absorption in the nuclear medium. This absorption, which is considered in the optical model through the imaginary part of the potential, leads to neutron emission (charge exchange), multinucleon and pion emission (resulting from hard interactions), redistribution of strength between residual nucleus states (a consequence of collective motion), etc. Clearly, all of these effects should be included in a full microscopic calculation. However, we considered inclusion of proton absorption effects in this analysis to be unwarranted in view of (i) the relatively large errors (statistical and propagated systematic) associated with the data after the L-T separation, (ii) the approximations involved in treating the data in terms of $p_m^{\rm eff}$, and (iii) the lack of a clear method to proceed.

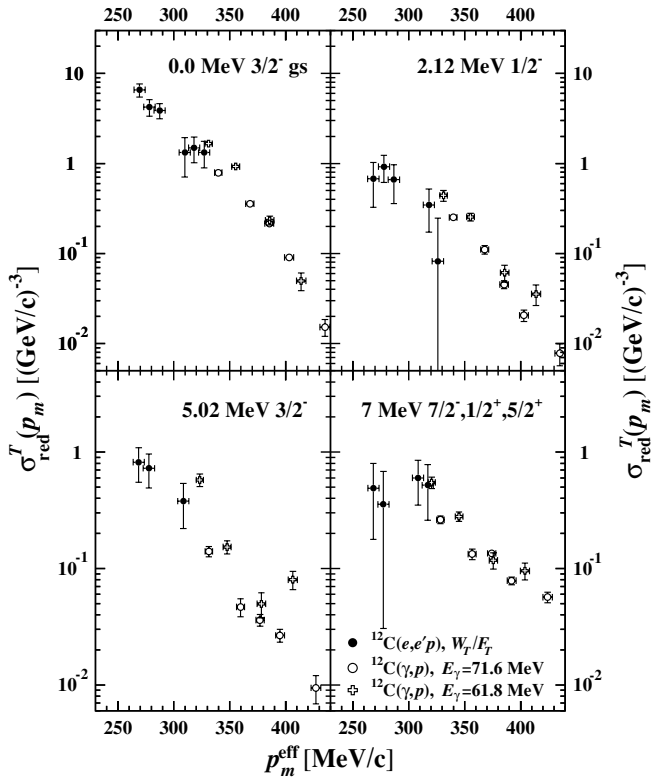


FIG. 9. Comparison of the transverse reduced cross sections for the present $(e, e'p)$ data with the four resolved transitions in the reaction $^{12}$C$(\gamma, p)$ data of Ruijter *et al*. [25], as a function of $p_m^{\text{eff}}$.

In considering Fig. 9, it should be noted that comparisons between the $^{12}$C$(e, e'p)^{11}$B and $^{12}$C$(\gamma, p)^{11}$B reactions have been made in the past (e.g., [8]) for $(e, e'p)$ data with $p_m < 220$ MeV/$c$. However, these comparisons did not focus on kinematic regions such that $p_m^{ee'p} \approx p_m^{\gamma p}$, nor did they use the purely transverse component of the $(e, e'p)$ cross section. From the results presented in Fig. 9, which do meet these conditions, it is evident that the transverse $(e, e'p)$ and $(\gamma, p)$ data connect reasonably smoothly and are fairly consistent where the data overlap.* The resulting distribution suggests that the transverse $(e, e'p)$ and the $(\gamma, p)$ reaction mechanisms are similar, although a definitive conclusion will clearly require better $^{12}$C$(e, e'p)^{11}$B data and a full calculation.

## VI. CONCLUSIONS

The electron-induced proton-knockout reaction on $^{12}$C has been studied in the $p_m$ range comparable to existing $(\gamma, p)$ data. Transitions to the $(3/2^-)_1$, $(1/2^-)$, $(3/2^-)_2$, and $(7/2^-, 1/2^+)$ doublet and the $(5/2^+)$ states of $^{11}$B have been resolved. A separation of the longitudinal and transverse structure functions has been performed, in parallel kinematics, for each of these transitions. The momentum distributions and separated structure functions have been compared with calculations based on the RPA model with and without the inclusion of MEC and IC contributions. The data have also been compared with CDWIA calculations constrained by previously measured $^{12}$C$(e, e'p)^{11}$B data at lower $p_m$.

The CDWIA calculations show that the DKO model underestimates the reduced cross sections for populations of the ∼7-MeV states in $^{11}$B. This result shows clearly that additional processes are required to describe the data for these states and is confirmed by the results of the RPA calculations including MEC and IC, which reproduce the cross sections for these states more closely. Figure 4 shows that this also applies to the $(1/2^-)$ state. Unfortunately, in the case of the structure functions, comparison between experiment and theory is not as conclusive as it is for the reduced cross sections, partly due to the increased error bars inherent in a Rosenbluth separation. For the $(1p)$-knockout transitions, the CDWIA and the RPA calculations both differ from the experimental cross sections, the difference being largest for the RPA calculations. The transitions to the triplet states show better agreement although, clearly, more accurate data are required before detailed conclusions can be drawn. The fact that the MEC and IC effects are required to account for the triplet states implies that the transverse $(e, e'p)$ and the $(\gamma, p)$ reactions proceed by similar mechanisms when restricted to identical kinematic conditions. This finding is in agreement with the conclusions of a comparison of similar calculations with experimental data for the $(\gamma, p)$ reaction [20]. In this case the experimental data were reproduced well.

For the first time, reduced cross sections for the transverse part of the reaction $^{12}$C$(e, e'p)$ have been compared with $^{12}$C$(\gamma, p)$ cross sections in the same $p_m$ range. All previous comparisons of these two reactions have involved $^{12}$C$(e, e'p)$ data measured at $p_m \leqslant 250$ MeV/$c$ and have included longitudinal contributions in the $(e, e'p)$ cross sections.

An effective missing momentum has been employed to minimize effects due to the different kinetic energy of the emitted proton, $T_p$, in each of the data sets. After calculation of this effective momentum, the $(\gamma, p)$ data are shifted to a higher $p_m$ (these data are affected more by the effective momentum because of their lower $T_p$), and the two reactions appear to show broad agreement. A smooth connection is observed for the transitions to the ground and 2.12-MeV states. The data for the 5.02-MeV transition are in agreement within the spread of the $(\gamma, p)$ data. Finally, there is no longer a large discrepancy between the two reactions for the transition to the ∼7-MeV states, as has been reported in previous comparisons [8]. A conclusion may be drawn even without considering how well the effective momentum accounts for the different FSI effects present in each of the two data sets. It is that all four transitions compare equally well, which implies that the two reactions proceed similarly when probed under similar kinematics. The ∼7-MeV states are now seen to compare almost as well as the other transitions. This has never been the case in previous comparisons [8] and was the driving motivation for this work.

*It goes beyond the scope of the present paper to discuss the differences between the two $^{12}$C$(\gamma, p)^{11}$B data sets shown.

**ACKNOWLEDGMENTS**

This work is part of the research program of the Stichting voor Fundamenteel Onderzoek der Materie (FOM), which is financially supported by the Nederlandse Organisatie voor Wetenschappelijk Onderzoek (NWO). The support of the UK Engineering and Physical Sciences Research Council is gratefully acknowledged.

[1] A. E. L. Dieperink and P. K. A. de Witt Huberts, Ann. Rev. Nucl. Part. Sci. **40**, 239 (1990).
[2] P. K. A. de Witt Huberts, J. Phys. G **16**, 507–544 (1990).
[3] G. van der Steenhoven, Nucl. Phys. **A527**, 17c (1991).
[4] L. Lapikás, Nucl. Phys. **A553**, 297c (1993).
[5] J. J. Kelly, Adv. Nucl. Phys. **23**, 75–294 (1996).
[6] D. Branford *et al*., Phys. Rev. C **63**, 014310 (2000), and references therein.
[7] E. C. Aschenauer *et al*., Phys. Lett. **B389**, 470 (1996).
[8] D. G. Ireland and G. van der Steenhoven, Phys. Rev. C **49**, 2182 (1994).
[9] L. J. de Bever *et al*., Phys. Rev. C **58**, 981 (1998).
[10] J. S. Levinger, Phys. Rev. **84**, 43 (1951); Phys. Lett. **B82**, 181 (1979).
[11] L. Van Hoorebeke *et al*., Phys. Rev. C **42**, R1179 (1990).
[12] D. A. Sims *et al*., Phys. Rev. C **45**, 479 (1992); L. Van Hoorebeke *et al*., *ibid.* **45**, 482 (1992).
[13] G. van der Steenhoven and H. P. Blok, Phys. Rev. C **42**, 2597 (1990).
[14] J. P. McDermott, E. Rost, J. R. Shepard, and C. Y. Cheung, Phys. Rev. Lett. **61**, 814 (1988).
[15] G. M. Lotz and H. S. Sherif, Nucl. Phys. **A537**, 285 (1992).
[16] J. I. Johansson, H. S. Sherif, and G. M. Lotz, Nucl. Phys. **A605**, 517 (1996).
[17] J. I. Johansson and H. S. Sherif, Phys. Rev. C **56**, 328 (1997).
[18] A. Meucci, C. Giusti, and F. D. Pacati, Phys. Rev. C **64**, 064615 (2001).
[19] J. Ryckebusch *et al*., Phys. Rev. C **46**, R829 (1992).
[20] A. Kuzin *et al*., Phys. Rev. C **58**, 2167 (1998).
[21] A. C. Shotter *et al*., Phys. Rev. C **37**, 1354 (1988).
[22] S. V. Springham *et al*., Nucl. Phys. **A517**, 93 (1990).
[23] D. G. Ireland *et al*., Nucl. Phys. **A554**, 173 (1993).
[24] A. W. Rauf, Ph.D. thesis, University of Edinburgh, 1996 (unpublished).
[25] H. Ruijter *et al*., Phys. Rev. C **54**, 3076 (1996).
[26] E. C. Aschenauer *et al*., Nucl. Phys. **A615**, 33 (1997).
[27] F. Ajzenberg–Selove, Nucl. Phys. **A506**, 1 (1990).
[28] S. A. Morrow, Ph.D. thesis, University of Edinburgh, 2000 (unpublished).
[29] T. de Forest Jr., Ann. Phys. (NY) **45**, 365 (1967).
[30] S. Boffi, C. Guisti, and F. D. Pacati, Nucl. Phys. **A386**, 599 (1982).
[31] S. Boffi, C. Giusti, and F. D. Pacati, Phys. Rep. **226**, 1 (1993).
[32] S. Boffi, F. Capuzzi, C. Giusti, and F. D. Pacati, Nucl. Phys. **A436**, 438 (1985).
[33] J. Ryckebusch, D. Debruyne, W. Van Nespen, and S. Janssen, Phys. Rev. C **60**, 034604 (1999).
[34] C. de Vries *et al*., Nucl. Instrum. Methods **223**, 1 (1984).
[35] P. K. A. de Witt Huberts, Nucl. Phys. **A553**, 845c (1993).
[36] E. N. M. Quint, Ph.D. thesis, Universiteit van Amsterdam, 1988 (unpublished).
[37] J. W. den Herder *et al*., Nucl. Phys. **A490**, 507 (1988).
[38] T. de Forest Jr., Nucl. Phys. **A392**, 232 (1983).
[39] C. M. Spaltro *et al*., Phys. Rev. C **48**, 2385 (1993).
[40] G. van der Steenhoven *et al*., Nucl. Phys. **A480**, 547 (1988); G. van der Steenhoven *et al*., *ibid.* **A484**, 445 (1988).
[41] L. Lapikás, G. van der Steenhoven, L. Frankfurt, M. Strikman, and M. Zhalov, Phys. Rev. C **61**, 064325 (2000).
[42] L. J. H. M. Kester *et al*., Phys. Lett. **B366**, 44 (1996).
[43] I. Bobeldijk, H. P. Blok, and G. van der Steenhoven, Phys. Lett. **B281**, 25 (1992).
[44] J. R. Comfort and B. C. Karp, Phys. Rev. C **21**, 2162 (1980).